ORIGINAL ARTICLE

Critical flux Richardson number for Kolmogorov turbulence enabled by TKE transport

Livia S. Freire[1] | **Marcelo Chamecki**[2] | **Elie Bou-Zeid**[3] | **Nelson L. Dias**[1,4]

[1]Graduate Program in Environmental Engineering, Federal University of Paraná, Curitiba PR, Brazil

[2]Department of Atmospheric and Oceanic Sciences, University of California, Los Angeles, CA, USA

[3]Department of Civil and Environmental Engineering, Princeton University, Princeton, NJ, USA

[4]Department of Environmental Engineering, Federal University of Paraná, Curitiba PR, Brazil

Correspondence
Livia S. Freire, Graduate Program in Environmental Engineering, Federal University of Paraná, Curitiba PR, Brazil
Email: liviagrion@gmail.com

Funding information

In stably stratified flows, the flux Richardson number Ri_f is a measure of the ratio between buoyancy destruction and shear production of turbulent kinetic energy (TKE). In flows with local equilibrium between shear production, buoyancy destruction and dissipation of TKE, the critical $Ri_{f,c} \approx 0.21$ corresponds to the limit above which Kolmogorov turbulence can no longer be sustained. Analysis of the TKE and velocity variance budget equations shows that the critical $Ri_{f,c}$ is increased by the presence of positive turbulent transport of TKE. This situation is observed, for example, in the roughness sublayer above plant canopies, as demonstrated using field data from the Amazon rainforest.

KEYWORDS
flux Richardson number, Kolmogorov turbulence, supercritical turbulence, stratified turbulence

1 | INTRUDUCTION

In stably stratified turbulent flows, the competing effects of shear and buoyancy are traditionally characterized by the gradient Richardson number $Ri_g = N^2/S^2$, where $N = \sqrt{(-g/\rho_0)(d\rho/dz)}$ is the Brunt-Väisälä frequency (g is gravitational acceleration, $\rho(z)$ is density, ρ_0 is a reference value and z is height) and $S = d\overline{u}/dz$ is the vertical shear of mean streamwise velocity $\overline{u}(z)$. Using linear stability analysis on steady, two-dimensional flow, Miles (1961) and Howard (1961) showed that Ri_g (assumed constant in space) has a critical value of 0.25 above which infinitesimal perturbations are damped. This definition, however, does not necessarily imply that turbulence is not sustained above this limit as turbulence has been observed at values of Ri_g up to 100 (Zilitinkevich et al., 2008). As other studies report turbulence

decay or growth suppression at certain values of Ri_g (Grachev et al., 2013), the existence of critical gradient Richardson number remains a controversial issue.

The flux Richardson number, on the other hand, does have a critical value observed from various laboratory experiment, large-eddy simulation (LES) and direct numerical simulation (DNS) (Zilitinkevich et al., 2010; Katul et al., 2014). Ri_f is defined as the ratio of buoyancy destruction ($-B$) to shear production (P) of turbulent kinetic energy (TKE). Although it is related to Ri_g by the turbulent Prandtl number ($Ri_g/Ri_f = Pr_t = K_M/K_H$, where K_H and K_M are the heat and momentum eddy diffusivities), the existence of a finite asymptotic value of Ri_f, while Ri_g remains unbounded, can be explained by the failure of the eddy diffusivity hypothesis: as the mean temperature gradient increases, the heat flux (and therefore $-B$) remains bounded by a counter-gradient flux due to the buoyancy effect of potential temperature fluctuations (Zilitinkevich et al., 2007).

From budget equations of TKE and density (or virtual temperature) variance, Ellison (1957) found $Ri_{f,c} \approx 0.15$ whereas Townsend (1958) obtained $Ri_{f,c} \approx 0.50$, the difference being caused by different closure assumptions (Yamada, 1975). Using velocity variance budget equations with the simplest linear Rotta closure model for return-to-isotropy terms (Rotta, 1951), and assuming isotropy for the velocity variance dissipation terms, Bou-Zeid et al. (2018) obtained $Ri_{f,c} = 0.21$. This is exactly equal to the value obtained by Mellor and Yamada (1974) and Yamada (1975) using analytical models for the full Reynolds stress tensor and temperature variance budgets, along with more detailed redistribution models. In all of these analyses, the usual assumptions of the canonical atmospheric surface layer (ASL) are invoked (stationarity, horizontal homogeneity, and negligible turbulent transport of TKE or velocity and scalar variances).

In the canonical ASL, the flux Richardson number is often presented in the framework of Monin-Obukhov Similarity Theory (MOST), and written in the form $Ri_f = \zeta\phi_m^{-1}(\zeta)$, where $\zeta = z/L$ is the stability parameter, z is the height above ground, L is the Obukhov length, and $\phi_m(\zeta)$ is the non-dimensional vertical gradient of mean streamwise velocity. Experimental data show that, in the stable ASL, $\phi_m(\zeta) = 1 + \beta\zeta$ with $\beta \approx 5$, resulting in an asymptotic $Ri_f \to 1/\beta \approx 0.2$ for $\zeta \to \infty$ (increasing stability) (Wyngaard, 2010, p. 281). This result provides an upper limit for Ri_f which is remarkably close to the critical value obtained from TKE and velocity variance budgets. Note that MOST also assumes steady-state and horizontally homogeneous conditions, and although it does not explicitly assume zero turbulent transport, the similarity functions obtained empirically correspond to a TKE budget in which most of the local production is balanced by local buoyant destruction and dissipation (Chamecki et al., 2018).

In spite of the consensus over $Ri_{f,c} \approx 0.20 - 0.25$ from theory and observations (Zilitinkevich et al., 2010), in the atmosphere this value is likely related to the assumptions of the canonical ASL. For example, Grachev et al. (2013) observed that a well-defined inertial subrange with a $-5/3$ slope on the energy spectrum (i.e., "Kolmogorov turbulence") was observed for Ri_f up to $0.20 - 0.25$ in the ASL over the Arctic. Differently, Babić and Rotach (2018) observed "Kolmogorov turbulence" in data with $Ri_f > 0.25$ from measurements in a deciduous canopy roughness sublayer, speculating that the cause might be associated with surface heterogeneity. Chamecki et al. (2018) noted a large number of data points in the range $0.25 < Ri_f < 1.5$ in the roughness sublayer above the Amazon forest, mostly in conditions for which local production was smaller than local dissipation of TKE (ϵ).

In this work, we hypothesize that turbulent transport of TKE can maintain "Kolmogorov turbulence" above $Ri_f \approx 0.20 - 0.25$. Extending the approach presented by Bou-Zeid et al. (2018), we derive a new $Ri_{f,c}$ that includes the TKE transport term. In the reduced TKE phase-space proposed by Chamecki et al. (2018), this defines a new region of *transport-enabled turbulence*. We use the same dataset presented by Chamecki et al. (2018) to test this hypothesis and characterize roughness-sublayer turbulence above a forest canopy in this regime.

2 | CRITICAL RICHARDSON NUMBER IN THE PRESENCE OF TURBULENT TRANSPORT

We start from the reduced TKE budget as defined by Chamecki et al. (2018), assuming that the turbulent transport of TKE is the sole responsible for the local production-dissipation imbalance (R), i.e,

$$\underbrace{-\overline{u'w'}\frac{d\overline{u}}{dz}}_{P}+\underbrace{\frac{g}{\overline{\theta_v}}\overline{w'\theta_v'}}_{B}-\epsilon=R\approx\underbrace{\frac{d\overline{w'e}}{dz}}_{-T_e}. \tag{1}$$

Similarly, we write the half-variance budget equations under stationary and horizontally-homogeneous conditions as

$$\underbrace{-\overline{u'w'}\frac{d\overline{u}}{dz}}_{P}\underbrace{-\frac{1}{2}\frac{d\overline{w'u'u'}}{dz}}_{T_u}+\underbrace{\overline{\frac{p'}{\rho_0}\frac{\partial u'}{\partial x}}}_{\Pi_u}-\epsilon_u=0, \tag{2}$$

$$\underbrace{-\frac{1}{2}\frac{d\overline{w'v'v'}}{dz}}_{T_v}+\underbrace{\overline{\frac{p'}{\rho_0}\frac{\partial v'}{\partial y}}}_{\Pi_v}-\epsilon_v=0, \tag{3}$$

$$\underbrace{\frac{g}{\overline{\theta_v}}\overline{w'\theta_v'}}_{B}\underbrace{-\frac{1}{2}\frac{d\overline{w'w'w'}}{dz}}_{T_w}+\underbrace{\overline{\frac{p'}{\rho_0}\frac{\partial w'}{\partial z}}}_{\Pi_w}-\epsilon_w=0, \tag{4}$$

where $e=(u'u'+v'v'+w'w')/2$ and $\overline{e}$ is the TKE, u, v and w are the streamwise, cross-stream and vertical velocity components, respectively, θ_v is virtual temperature, ρ_0 is a reference density, p is pressure, and ϵ, ϵ_u, ϵ_v and ϵ_w are the dissipation rates of TKE and half-variance components, respectively. Overbar and primes represent ensemble mean and fluctuation, respectively. To simplify notation, hereafter we use P for shear production, B for buoyancy production/destruction, T for the turbulent transport and Π for pressure redistribution, as indicated in Equations (4)–(4).

As proposed by Bou-Zeid et al. (2018), by summing Equations (2) and (3), assuming an approximately isotropic dissipation rate to write

$$\epsilon_u+\epsilon_v=2\epsilon_w, \tag{5}$$

and using Equation (4) to replace ϵ_w, all three variance equations can be combined into one equation given by

$$P+T_u+T_v+\Pi_u+\Pi_v=2B+2T_w+2\Pi_w. \tag{6}$$

Because the pressure redistribution terms add up to zero, i.e.,

$$\Pi_u+\Pi_v=-\Pi_w, \tag{7}$$

this equation can be further reduced into

$$P+T_u+T_v-2T_w-3\Pi_w=2B, \tag{8}$$

or, rewriting it,

$$\frac{\Pi_w}{P} + \frac{2T_w - T_u - T_v}{3P} = \frac{1}{3} + \frac{2}{3} Ri_f, \tag{9}$$

where $Ri_f = -B/P$ is the flux Richardson number.

Following Mellor and Yamada (1974) and Bou-Zeid et al. (2018), a linear Rotta-type closure is adopted for the pressure redistribution term (Rotta, 1951; Davidson, 2004), namely

$$\Pi_w = -\frac{c\epsilon}{\overline{e}} \left(\overline{w'w'} - \frac{2}{3}\overline{e} \right). \tag{10}$$

This closure is used in Equation (9), which is then combined with Equation (4) in the form

$$\epsilon/P = 1 - Ri_f + T_e/P, \tag{11}$$

resulting in

$$\frac{\overline{w'w'}}{\overline{e}} = -\frac{1}{3c} \left[\frac{1 + 2Ri_f - 3T_w/P + T_e/P}{1 - Ri_f + T_e/P} \right] + \frac{2}{3}. \tag{12}$$

This relationship between $\overline{w'w'}$ and Ri_f reveals a critical value of Ri_f over which $\overline{w'w'}$ would become negative, and the constraint of $\overline{w'w'} > 0$ yields a constraint on Ri_f

$$Ri_f < \frac{2c-1}{2c+2} + \frac{3}{2c+2}\frac{T_w}{P} + \frac{2c-1}{2c+2}\frac{T_e}{P}. \tag{13}$$

In the absence of turbulent transport (i.e. $T_e = T_w = 0$) and adopting $c = 0.9$ for the closure constant of the Rotta model, this equation yields a critical Richardson number $Ri_{f,c} \approx 0.21$ (Bou-Zeid et al., 2018). For positive transport, this critical value is enhanced by the ratios T_w/P and T_e/P, allowing turbulence to be sustained under stronger stratification. Equation (13) can be simplified even further by assuming $T_w = \alpha T_e$ (see Figure S1 in the Supporting Information), which gives

$$Ri_f < \frac{2c-1}{2c+2} + \frac{3\alpha + 2c - 1}{2c+2}\frac{T_e}{P}. \tag{14}$$

For positive net TKE turbulent transport $T_e > 0$ (implying its vertical gradient in Equation (4) is negative and it is thus a source that augments TKE), Equation (14) provides a transport-enhanced critical flux Richardson number. If the values $c = 0.9$ (Katul et al., 2013) and $\alpha = 0.28$ (valid for the present data, see Figure S1) are used, this yields a critical flux Richardson number

$$Ri_{f,c} \approx 0.21 + 0.43\, T_e/P. \tag{15}$$

It is important to note that Rotta's model (Equation (10)) is the simplest closure available for the pressure redistribution term, representing only the slow part of the process (Davidson, 2004). In the presence of large mean velocity gradients, such as for flow above pant canopies, fast redistribution terms can also be important (e.g., see Launder et al., 1975). For simplicity and generality, we focus on first-order effects and use only the slow component here.

3 | FIELD DATA

Data from the GoAmazon experiment (Fuentes et al., 2016) are used to test the existence of turbulence and its characteristics in the transport-enabled region predicted by Eqn. (14). This dataset consists of wind velocity (three components) and virtual temperature measured at 20 Hz by nine sonic anemometers (model CSAT3, Campbell Scientific Inc, Logan, UT) mounted on a 50 m tower in the Amazon rainforest. Measurement heights correspond to $z/h = 0.20, 0.39, 0.52, 0.63, 0.70, 0.90, 1.00, 1.15$ and 1.38, where $h = 35$ m is the approximate canopy height. Data were collected continuously between March 2014 and January 2015 and separated in blocks of 30-min starting at 00:00 local time. Blocks with more than 1 second of consecutive error flags were discarded, and the remaining missing values were replaced by the previous measurement. A planar fit for the entire data set was performed to correct for instrument tilting (Wilczak et al., 2001), using blocks with mean wind direction at the highest anemometer within $\pm 90^\circ$ of the instrument axis (the remaining blocks were discarded). Blocks with negative heat flux at $z/h = 1$ were filtered with a 3-min top-hat high-pass filter, to eliminate non-turbulent oscillations that can be significant under stably stratified conditions (Mahrt, 2014). Using the criteria proposed by Vickers and Mahrt (1997), blocks with non-stationary ratios larger than or equal to 0.5 were discarded. Blocks were further selected by the existence of an inertial subrange in the second-order longitudinal structure function with slope within 10% of the theoretical prediction of 2/3 (Kolmogorov, 1941), estimated in the range $0.5 \leq r \leq 2$ m, which was then used to infer TKE dissipation rates via $\overline{\Delta u^2} = C_2(r\epsilon)^{2/3}$ with $C_2 = 1.97$ following Chamecki and Dias (2004). A time-varying displacement height d_0 was estimated from measurements of momentum flux inside the canopy (Pan and Chamecki, 2016) and blocks with $d_0 < 0$ or $d_0 > h$ were also discarded. A total of 850 blocks from each height remained for the present analysis.

The data analyses focus on turbulence in the roughness sublayer above the forest, i.e. at $z/h \geq 1$. Therefore, mean velocity gradients needed to estimate the shear production were determined using a second-order polynomial fit in $\ln(z)$ (Högström, 1988) using data from the four upper anemometers, as they follow an approximately logarithmic profile (see Chamecki et al. (2018) for examples). To estimate turbulent transport of TKE, a second-order polynomial fit in z was adjusted to the TKE vertical flux $\overline{w'e}$ from the upper three anemometers, because fluxes at $z/h = 0.90$ did not always conform with the curvature of the upper three anemometers. Although it is not possible to assess the quality of the fit (as these are fits of second-order polynomials to three data points), the overall agreement with the literature on canopy flows serves as an indirect indication that the fits are reasonable.

4 | RESULTS

To establish confidence in our dataset and provide a basis for comparison, we first look at results under near-neutral conditions (defined as $|Ri_f| < 0.04$ at $z/h = 1.38$). In this case, the normalized shear length scale $L_s/h = [\overline{u}(h)/(d\overline{u}/dz)_h]/h$ is on average 0.47, which is typical for forest environments (Finnigan, 2000). The TKE increases monotonically with height, with a very large gradient in the upper half of the canopy (Figure 1-a). This produces a turbulent flux of TKE that is predominantly negative inside the canopy and positive above (Figure 1-b), with a positive gradient where $z/h > 1$. Thus, in agreement with current understanding of canopy flows in neutral conditions (Finnigan, 2000), we observe net turbulent transport of TKE into the canopy region ($T_e < 0$ for $z/h > 1$, Figure 1-c). This leads to an imbalance between local production and dissipation above the canopy ($P/\epsilon > 1$), which decreases with height reaching a nearly balanced state at the transition between the roughness sublayer and the surface layer above (Pan and Chamecki, 2016). Under stable conditions, the shear length scale is reduced, on average, to $L_s/h = 0.34$, suggesting less penetration of shear layer eddies into the canopy. However, the main feature of interest here is that the TKE profile is no longer monotonic in

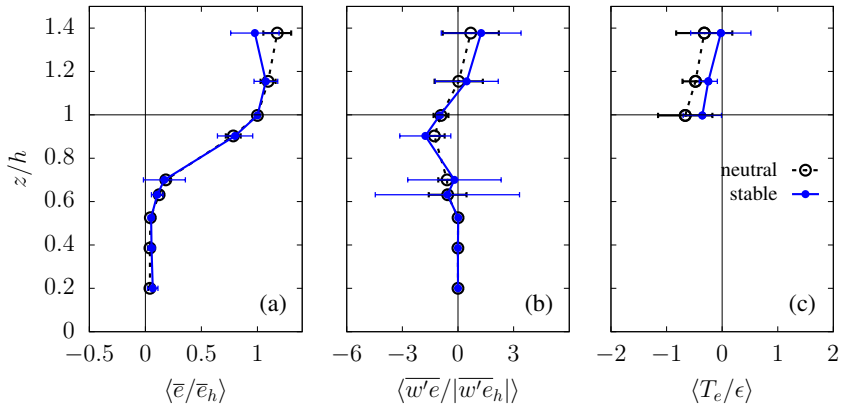

FIGURE 1 Vertical profiles of normalized (a) TKE, (b) turbulent flux of TKE, and (c) net vertical turbulent transport of TKE for neutral conditions ($|Ri_f| < 0.04$ at $z/h = 1.38$, open, black symbols) and stable conditions ($Ri \geq 0.04$ at $z/h = 1.38$, closed, blue symbols). Circles represent averages over data blocks and error bars represent one standard deviation. The TKE turbulent transport was estimated from a second-order polynomial fit to the turbulent flux of TKE above canopy (three uppermost points).

the near-canopy region, displaying a clear maximum at canopy top. This leads to predominantly positive net turbulent transport of TKE far above the canopy (at $z/h = 1.38$, Figure 1-c), so that here $(P + B)/\epsilon < 1$, as observed by Chamecki et al. (2018). Although this particular feature has not yet been discussed in the literature, it has also been observed above deciduous forests (Leclerc et al., 1990; Babić and Rotach, 2018). In the present study, the existence of this region with positive net transport of TKE is connected to the existence of Kolmogorov turbulence with $Ri_f > 0.21$, as discussed next.

As an initial step in exploring the relationship between flux Richardson number and turbulent transport of TKE, Figure 2-a presents the normalized transport T_e/ϵ and residual R/ϵ (Eqn.) versus Ri_f, for the data measured above the forest ($z/h \geq 1$). Despite the large scatter, it is quite remarkable how clearly the line $Ri_f = 0.21$ separates points with positive transport from points with negative transport, on average. It is also clear that, on average, the turbulent transport of TKE is responsible for a significant portion of the imbalance between local production and dissipation of TKE. Figure 2-b shows the increase of kurtosis of streamwise and vertical velocity with Ri_f in the stable case, indicating an increase in the importance of strong events as stability increases.

To demonstrate more clearly the relationship between flux Richardson number and transport of TKE, the same data are displayed on the TKE phase space developed by Chamecki et al. (2018) in Figure 3. This two-dimensional diagram presents data points according to P/ϵ and B/ϵ, and the local imbalance between TKE production and dissipation is proportional to the distance to the local balance line (indicated in Figure 3 by the black solid line given by $B + P = \epsilon$). The diagram also explicitly shows the value of Ri_f as straight lines emanating from the origin (lines of constant Ri_f increasing clockwise). The runs with $Ri_f > 0.21$ present very large normalized TKE ($\bar{e}/u_s^2$, where u_s is the local friction velocity) and predominantly positive net turbulent transport of TKE (Figures 3-a and 3-b, respectively). These results suggest that the large TKE content in this region of the phase space is not associated with local production, but rather it is transported by turbulence from elsewhere (note that non-turbulent variance typically observed under stable conditions have been removed by the 3-min high-pass filter used for stable runs). Thus, turbulent transport seems to sustain turbulence in stratified environments with $Ri_f > 0.21$.

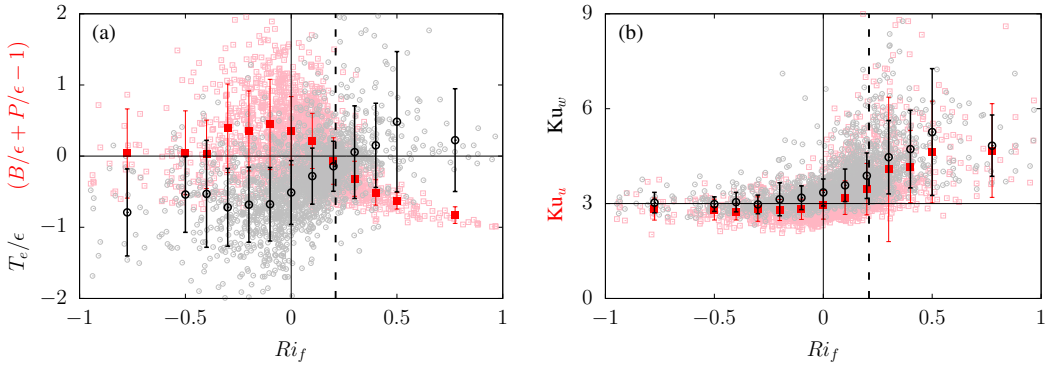

FIGURE 2 (a) Normalized local imbalance between production and dissipation of TKE (red squares) and turbulent transport of TKE (black circles) displayed as a function of the flux Richardson number Ri_f. (b) Kurtosis of streamwise (Ku_u) and vertical (Ku_w) velocities as a function of the flux Richardson number. Symbols represent ensemble averages conditioned on Ri_f and errorbars represent one standard deviation. Dashed line indicates $Ri_f = 0.21$.

Given that transport can maintain turbulence above $Ri_f = 0.21$, it is of interest to delineate this region in the TKE phase space. In order to do so, we must assume that the local imbalance between production and dissipation is only caused by turbulent transport so that Eqn. (4) can be used in the form $T_e/\epsilon = 1 - B/\epsilon - P/\epsilon$ to rewrite Equation (14) as

$$\frac{B}{\epsilon} > \frac{\alpha}{(1-\alpha)}\frac{P}{\epsilon} + \frac{1-3\alpha-2c}{3-3\alpha}. \tag{16}$$

Equation (16) is displayed on the diagram, marking the region where turbulent transport is enough to sustain turbulence (Figure 3-c). However, Eqn. (4) is only approximately satisfied by the observations, as the turbulent transport is estimated independently from the imbalance (other potential sources of imbalance are non-stationarity, mean advection, and pressure transport). Hereafter, we restrict our analysis to the runs in which turbulent transport is a significant portion of the total imbalance. We define the parameter

$$\eta = \frac{(R + T_e)^2}{R^2 + T_e^2}, \tag{17}$$

which is a measure of the fraction of the imbalance accounted for by the turbulent transport. Note that by construction $0 \leq \eta \leq 2$, with $\eta = 0$ implying that all the imbalance is caused by transport ($-T_e = R$). The distribution of η for the GoAmazon data can be found in the Supporting Information (Figure S2). From here on we restrict the data analysis to runs with $\eta \leq 0.2$, which ensures that transport is at least 50% of the total imbalance ($-T_e \geq 0.5R$).

Most of the remaining runs (68 of the 86 runs with $Ri_f > 0.21$) fall in the region of transport-enabled turbulence as predicted by Eqn. (14) (Figure 3-c). All these points have positive net transport as expected. This result does not depend on the choice of $c = 0.9$, as the change in $Ri_{f,c}$, as well as the change in the region of transport-enabled turbulence, is small for $0.8 \leq c \leq 1$ (see Figure 3-c). As imposed by the data selection criterion, all points shown in Figure 3-c present a well-defined inertial subrange with a 2/3 slope region in the second-order structure function of streamwise velocity (Figure 4). An inertial subrange is also clearly present in the vertical velocity structure function, and no appreciable differences are found in the structure functions for transport-enabled turbulence and other stable runs with $Ri_f < 0.21$. Thus, we can conclude that the turbulence maintained by turbulent transport in the yellow region of the diagram

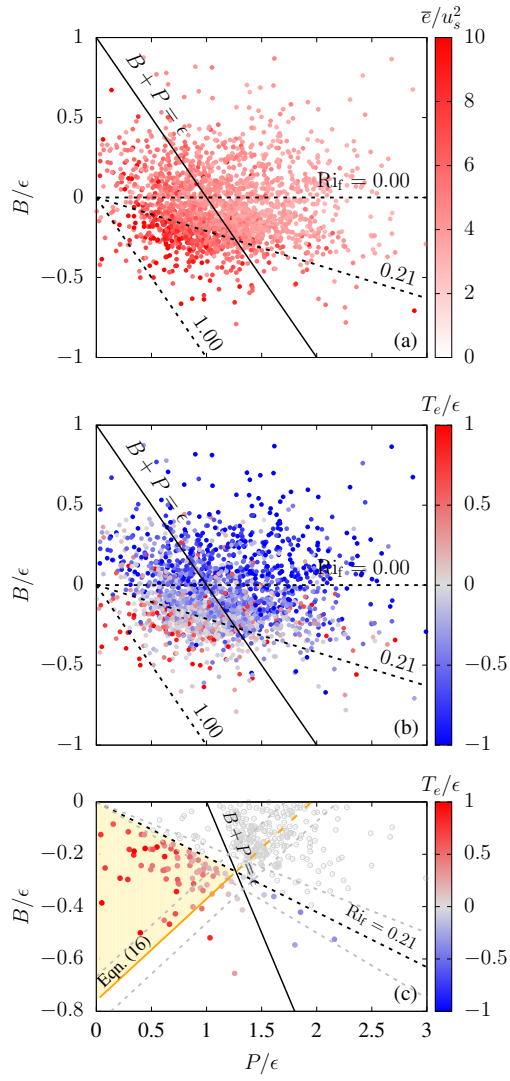

FIGURE 3 Data from $z/h \geq 1$ displayed on the TKE phase space, color-coded based on value of (a) TKE normalized by local friction velocity ($\overline{e}/u_s^2$) and (b) turbulent transport of TKE normalized by local dissipation rate (T_e/ϵ). (c) Same as (b) but including only data for $B < 0$. Orange line represents Equation (16) for $c = 0.9$, yellow region represents the transport-enabled region, and grey lines represent $Ri_{f,c}$ and Equation (16) for $c = 0.8$ and 1. Only points with $\eta \leq 0.2$ are displayed in (c).

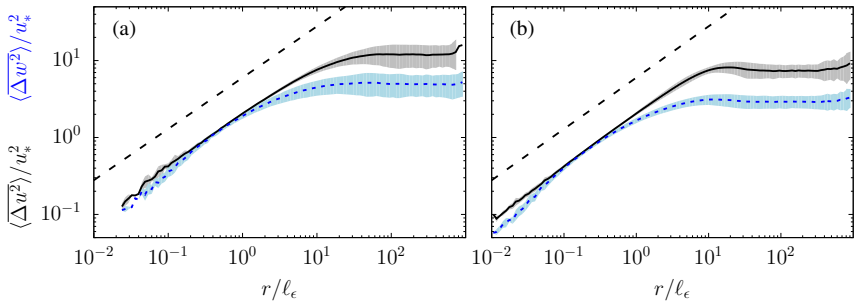

FIGURE 4 Second-order structure function of streamwise velocity (black, solid line) and vertical velocity (blue, dashed line) normalized by the friction velocity at canopy top (u_*) and the dissipation-based length scale $\ell_\epsilon = u_*^3/\epsilon$ (Pan and Chamecki, 2016). Results are shown for (a) transport-enabled turbulence (68 runs) and (b) stable runs with $0.04 \leq Ri_f \leq 0.21$ (211 runs). Thick line is the average of all points in the transport enabled region, and shaded area is one standard deviation. Dashed straight line corresponds to the 2/3 slope. Note that the data was high-pass filtered before calculation of structure functions, which impacts the large scales of streamwise velocity (see Figure S4 in the Supporting information).

displays a clear "Kolmogorov" energy cascade. This is in contrast to the surface layer results reported by Grachev et al. (2013), where large TKE transport is likely not present. Note, however, that the value of $\overline{\Delta w^2}/\overline{\Delta u^2} \approx 1$ in the inertial subrange indicates that the portion of the inertial subrange sampled in these data deviates from local isotropy (local isotropy implies a ratio of 4/3 (Pope, 2000)). Ratios $\overline{\Delta w^2}/\overline{\Delta u^2} \approx 1$ have also been observed in the ASL by Chamecki and Dias (2004) and Chamecki et al. (2018), and in the roughness sublayer by Babić and Rotach (2018). Even though the evidence for anisotropy within the inertial subrange of atmospheric turbulence is building up, further investigation is needed to discard other possibilities. At this point, it is not clear if local isotropy will be reached at scales smaller than the ones typically sampled by sonic anemometers or if these sensors introduce distortions in the flow field that lead to anisotropic ratios. Finally, the remaining 18 runs, which are outside the transport-enabled region, also display a clear inertial subrange, and the existence of Kolmogorov turbulence in these runs cannot be explained by turbulent transport of TKE (as $Ri_f > Ri_{f,c}$).

Although turbulence with $Ri_f > 0.21$ is sustained by transport rather than by local production alone, it does not present distinct characteristics from typical turbulence in the stable ABL. Visual inspection of time series of vertical velocity (not shown) suggest that most runs are characterized by continuous turbulence, with very few runs (both above and below the limit $Ri_{f,c} = 0.21$) displaying mild global intermittency. Runs with stronger global intermittency, typically observed in strongly stratified surface layers (e.g., as shown in Sun et al., 2002, 2004), were removed from our analyses by the stationarity tests applied. We do not observe any trend in the nonstationarity ratios with Ri_f (see Figure S3 in the Supporting information), confirming that the transport-enabled turbulence identified in the present data is an equilibrium state unlike the decaying turbulence observed during periods of increasing stratification by Grachev et al. (2013). Perhaps the most distinct feature of the turbulence at elevated values of Ri_f is the increase in the kurtosis of streamwise and vertical velocity components (Figure 2-b). This departure from gaussianity, which is expected in stably stratified turbulence (Chu et al., 1996; Ferrero and Anfossi, 1998), increases gradually with increasing Ri_f, and does not suggest a sharp transition in behavior at the onset of transport-enabled turbulence.

5 | CONCLUSION

A simple analysis of the budgets for the TKE and variances of the velocity components, with conventional closure assumptions but including the turbulent transport of TKE, reveals that the critical flux Richardson number for existence of Kolmogorov turbulence can be increased by positive turbulent transport (as compared to the case with negligible transport for which $Ri_{f,c} \approx 0.21$). In the TKE phase space, this leads to a well-defined region of transport-enabled turbulence. Data in the canopy roughness sublayer collected over the Amazon rainforest displays a region of positive transport under stable conditions. We show that, for data selected based on the existence of a Kolmogorov inertial subrange, transport becomes positive around $Ri_f \approx 0.21$. For the cases in which the transport corresponds to at least half of the imbalance between TKE local production and dissipation, the transport explains the existence of Kolmogorov turbulence in 79% of the 86 runs with $Ri_f > 0.21$. This result confirms our initial hypothesis that in flows where turbulent transport of TKE is positive, Kolmogorov turbulence can be sustained under stronger stable stratifications than previously assumed.

ACKNOWLEDGEMENTS

L.S.F. and N.L.D. were funded by the Brazilian National Council for Scientific and Technological Development (CNPq), under contracts 150769/2017-2 and 301420/2017-3, respectively. M.C. acknowledges partial funding from the National Science Foundation (grant AGS-1644375). E.B.Z. was supported by the Princeton Environmental Institute's Grand Challenges Program. The processed data needed for reproducing the figures are available from the authors upon request (chamecki@ucla.edu).

SUPPORTING INFORMATION

The following supporting information is available as part of the online article:

Figure S1. Relation between turbulent transport of vertical half-variance (T_w) and TKE (T_e) for the GoAmazon data.

Figure S2. Probability density function (PDF) of parameter η for the GoAmazon data.

Figure S3. Non-stationarity ratios displayed on the reduced TKE phase space.

Figure S4. Second-order structure function of streamwise velocity and vertical velocity prior to high-pass filter.

REFERENCES

Babić, K. and Rotach, M. W. (2018) Turbulence kinetic energy budget in the stable boundary layer over a heterogeneous surface. *Quarterly Journal of the Royal Meteorological Society*, **144**, 1045–1062. URL: https://rmets.onlinelibrary.wiley.com/doi/abs/10.1002/qj.3274.

Bou-Zeid, E., Gao, X., Ansorge, C. and Katul, G. G. (2018) On the role of return-to-isotropy in wall-bounded turbulent flows with buoyancy. *Journal of Fluid Mechanics*. URL: http://dx.doi.org/10.1017/jfm.2018.693.

Chamecki, M. and Dias, N. L. (2004) The local isotropy hypothesis and the turbulent kinetic energy dissipation rate in the atmospheric surface layer. *Quarterly Journal of the Royal Meteorological Society*, **130**, 2733–2752. URL: http://dx.doi.org/10.1256/qj.03.155.

Chamecki, M., Dias, N. L. and Freire, L. S. (2018) A TKE-based framework for studying disturbed atmospheric surface layer flows and application to vertical velocity variance over canopies. *Geophysical Research Letters*, **45**, 6734–6740. URL: https://doi.org/10.1029/2018GL077853.

Chu, C. R., Parlange, M. B., Katul, G. G. and Albertson, J. D. (1996) Probability density functions of turbulent velocity and temperature in the atmospheric surface layer. *Water Resources Research*, **32**, 1681–1688. URL: https://agupubs.onlinelibrary.wiley.com/doi/abs/10.1029/96WR00287.

Davidson, P. (2004) *Turbulence, an Introduction for scientists and engineerers*. Oxford University Press.

Ellison, T. H. (1957) Turbulent transport of heat and momentum from an infinite rough plane. *Journal of Fluid Mechanics*, **2**, 456–466. URL: http://dx.doi.org/10.1017/S0022112057000269.

Ferrero, E. and Anfossi, D. (1998) Comparison of pdfs, closure schemes and turbulence parameterisations in lagrangian stochastic models. *International Journal of Environment and Pollution*, **9**, 384–410. URL: https://www.inderscienceonline.com/doi/abs/10.1504/IJEP.1998.028253.

Finnigan, J. (2000) Turbulence in plant canopies. *Annual Review of Fluid Mechanics*, **32**, 519–571. URL: http://dx.doi.org/10.1146/annurev.fluid.32.1.519.

Fuentes, J. D., Chamecki, M., dos Santos, R. M. N., Randow, C. V., Stoy, P. C., Katul, G., Fitzjarrald, D., Manzi, A., Gerken, T., Trowbridge, A., Freire, L. S., Ruiz-Plancarte, J., Maia, J. M. F., Tóta, J., Dias, N., Fisch, G., Schumacher, C., Acevedo, O. and Mercer, J. R. (2016) Linking meteorology, turbulence, and air chemistry in the amazon rainforest. *Bulletin of the American Meteorological Society*, **97**, 2329–2342. URL: http://dx.doi.org/10.1175/BAMS-D-15-00152.1.

Grachev, A. A., Andreas, E. L., Fairall, C. W., Guest, P. S. and Persson, P. O. G. (2013) The critical richardson number and limits of applicability of local similarity theory in the stable boundary layer. *Boundary-Layer Meteorology*, **147**, 51–82. URL: https://doi.org/10.1007/s10546-012-9771-0.

Högström, U. (1988) Non-dimensional wind and temperature profiles in the atmospheric surface layer: A re-evaluation. *Boundary-Layer Meteorology*, **42**, 55–78. URL: https://doi.org/10.1007/BF00119875.

Howard, L. N. (1961) Note on a paper of john w. miles. *Journal of Fluid Mechanics*, **10**, 509–512. URL: http://dx.doi.org/10.1017/S0022112061000317.

Katul, G. G., Porporato, A., Manes, C. and Meneveau, C. (2013) Co-spectrum and mean velocity in turbulent boundary layers. *Physics of Fluids*, **25**, 091702.

Katul, G. G., Porporato, A., Shah, S. and Bou-Zeid, E. (2014) Two phenomenological constants explain similarity laws in stably stratified turbulence. *Phys. Rev. E*, **89**, 023007. URL: https://link.aps.org/doi/10.1103/PhysRevE.89.023007.

Kolmogorov, A. N. (1941) The local structure of turbulence in incompressible viscous fluid for very large reynolds numbers. *Proceedings: Mathematical and Physical Sciences*, **434**, 9–13. URL: http://www.jstor.org/stable/51980.

Launder, B. E., Reece, G. J. and Rodi, W. (1975) Progress in the development of a reynolds-stress turbulence closure. *Journal of Fluid Mechanics*, **68**, 537–566.

Leclerc, M. Y., Shaw, R. H., Hartog, G. D. and Neumann, H. H. (1990) The influence of atmospheric stability on the budgets of the reynolds stress and turbulent kinetic energy within and above a deciduous forest. *Journal of Applied Meteorology*, **29**, 916–933. URL: https://doi.org/10.1175/1520-0450(1990)029<0916:TIOASO>2.0.CO;2.

Mahrt, L. (2014) Stably stratified atmospheric boundary layers. *Annual Review of Fluid Mechanics*, **46**, 23–45. URL: http://dx.doi.org/10.1146/annurev-fluid-010313-141354.

Mellor, G. L. and Yamada, T. (1974) A hierarchy of turbulence closure models for planetary boundary layers. *Journal of the Atmospheric Sciences*, **31**, 1791–1806. URL: https://doi.org/10.1175/1520-0469(1974)031<1791:AHOTCM>2.0.CO;2.

Miles, J. W. (1961) On the stability of heterogeneous shear flows. *Journal of Fluid Mechanics*, **10**, 496–508. URL: http://dx.doi.org/10.1017/S0022112061000305.

Pan, Y. and Chamecki, M. (2016) A scaling law for the shear-production range of second-order structure functions. *Journal of Fluid Mechanics*, **801**, 459–474. URL: http://dx.doi.org/10.1017/jfm.2016.427.

Pope, S. B. (2000) *Turbulent Flows*. Cambridge University Press.

Rotta, J. (1951) Statistische theorie nichthomogener turbulenz. *Zeitschrift für Physik*, **129**, 547–572. URL: https://doi.org/10.1007/BF01330059.

Sun, J., Burns, S. P., Lenschow, D. H., Banta, R., Newsom, R., Coulter, R., Frasier, S., Ince, T., Nappo, C., Cuxart, J. et al. (2002) Intermittent turbulence associated with a density current passage in the stable boundary layer. *Boundary-Layer Meteorology*, **105**, 199–219.

Sun, J., Lenschow, D. H., Burns, S. P., Banta, R. M., Newsom, R. K., Coulter, R., Frasier, S., Ince, T., Nappo, C., Balsley, B. B. et al. (2004) Atmospheric disturbances that generate intermittent turbulence in nocturnal boundary layers. *Boundary-layer meteorology*, **110**, 255–279.

Townsend, A. A. (1958) Turbulent flow in a stably stratified atmosphere. *Journal of Fluid Mechanics*, **3**, 361–372. URL: http://dx.doi.org/10.1017/S0022112058000045.

Vickers, D. and Mahrt, L. (1997) Quality control and flux sampling problems for tower and aircraft data. *Journal of Atmospheric and Oceanic Technology*, **14**, 512–526. URL: https://doi.org/10.1175/1520-0426(1997)014<0512:QCAFSP>2.0.CO;2.

Wilczak, J., Oncley, S. and Stage, S. (2001) Sonic anemometer tilt correction algorithms. *Boundary-Layer Meteorology*, **99**, 127–150. URL: http://dx.doi.org/10.1023/A%3A1018966204465.

Wyngaard, J. C. (2010) *Turbulence In The Atmosphere*. Cambridge University Press.

Yamada, T. (1975) The critical richardson number and the ratio of the eddy transport coefficients obtained from a turbulence closure model. *Journal of the Atmospheric Sciences*, **32**, 926–933. URL: https://doi.org/10.1175/1520-0469(1975)032<0926:TCRNAT>2.0.CO;2.

Zilitinkevich, S. S., Elperin, T., Kleeorin, N. and Rogachevskii, I. (2007) Energy- and flux-budget (efb) turbulence closure model for stably stratified flows. part i: steady-state, homogeneous regimes. *Boundary-Layer Meteorology*, **125**, 167–191. URL: https://doi.org/10.1007/s10546-007-9189-2.

Zilitinkevich, S. S., Elperin, T., Kleeorin, N., Rogachevskii, I., Esau, I., Mauritsen, T. and Miles, M. W. (2008) Turbulence energetics in stably stratified geophysical flows: Strong and weak mixing regimes. *Quarterly Journal of the Royal Meteorological Society*, **134**, 793–799. URL: http://dx.doi.org/.

Zilitinkevich, S. S., Esau, I., Kleeorin, N., Rogachevskii, I. and Kouznetsov, R. D. (2010) On the velocity gradient in stably stratified sheared flows. part 1: Asymptotic analysis and applications. *Boundary-Layer Meteorology*, **135**, 505–511. URL: https://doi.org/10.1007/s10546-010-9488-x.